Journal of Alloys and Compounds 501 (2010) 37–41

Contents lists available at ScienceDirect

Journal of Alloys and Compounds

journal homepage: www.elsevier.com/locate/jallcom

Effect of zinc substitution on structural and magnetic properties of copper ferrite

P.P. Hankare[a,*], M.R. Kadam[a], R.P. Patil[a], K.M. Garadkar[a], R. Sasikala[b], A.K. Tripathi[b]

[a] Department of Chemistry, Shivaji University, Kolhapur 416004, India
[b] Chemistry Division, Bhabha Atomic Research Center, Mumbai 400085, India

ARTICLE INFO

Article history:
Received 4 October 2009
Received in revised form 18 March 2010
Accepted 21 March 2010
Available online 27 March 2010

Keywords:
: Ferrites
X-ray diffraction
Magnetization
SEM and EDAX

ABSTRACT

The Cu–Zn mixed ferrites viz. $Cu_{1-x}Zn_xFe_2O_4$ ($x = 0$, 0.25, 0.50, 0.75 and 1.0) were synthesized by the oxalate co-precipitation method. Formation of the cubic ferrite phase was confirmed by X-ray diffraction studies. Microstructural and compositional features were studied by scanning electron microscopy and energy dispersive X-ray analysis technique. Magnetic properties were measured by B–H hystersis loop tracer technique. The variation of saturation magnetization, remanent magnetization and coercivity were studied as a function of zinc content. The substitution of zinc ions plays decisive role in changing structural and magnetic properties of copper ferrite.

1. Introduction

Spinel ferrites have potential applications as electrical components such as memory and microwave devices due to their high resistivity and low loss eddy current [1–5]. In the recent years, nanosized spinel ferrites have attracted considerable attention for their interesting structural, magnetic and electrical properties. Copper ferrite has potential applications in nanoscience and technology. Non-magnetic Zn doped copper ferrites are of interest in fundamental understanding of the properties and variety of applications such as radiofrequency circuits, transformer cores, antennas and read/write heads for high speed digital tape and in high quality filters [6–9].

In the present investigation, an attempt has been made to study the structural, magnetic and microstructural properties of $Cu_{1-x}Zn_xFe_2O_4$ ferrites with $x = 0.0$, 0.25, 0.5, 0.75, 1.0. We report here, the synthesis of ferrites by the new chemical route like oxalate co-precipitation method [10] and their characterization using X-ray diffraction, scanning electron micrograph, EDAX measurements and magnetization.

2. Experimental

2.1. Sample preparation

The mixed metal oxide system $Cu_{1-x}Zn_xFe_2O_4$ with $x = 0.0$, 0.25, 0.50, 0.75 and 1.0 was prepared by oxalate co-precipitation method. Initially, stoichiometric amount of high purity AR grade copper sulphate, zinc sulphate and ferrous sulphate were carefully dissolved in doubly distilled water. The precipitation was carried out by adding 10% oxalic acid solution till the pH reaches 4.7.The chemical reactions proceed as follows:

$$CuSO_4 + 2H_2O + C_2O_4^{2-} \rightarrow CuC_2O_4{\cdot}2H_2O + SO_4^{2-}$$

$$ZnSO_4 + 2H_2O + C_2O_4^{2-} \rightarrow ZnC_2O_4{\cdot}2H_2O + SO_4^{2-}$$

$$FeSO_4 + 2H_2O + C_2O_4^{2-} \rightarrow FeC_2O_4{\cdot}2H_2O + SO_4^{2-}$$

The reaction mixture was heated on water bath for 4 h. The precipitate was filtered and washed several times with double distilled water to remove excess acid and sulphate ions with barium nitrate test. The compounds were dried at 110 °C in an oven and finally sintered at 900 °C for 6 h. The sintered powders were mixed with 2% polyvinyl alcohol as a binder and uniaxially pressed at a pressure of 8 tons/cm^2 to form pellets. These pellets were gradually heated to about 773 K to remove the organic binder material.

2.2. Characterization

The phase formation of the samples was confirmed by X-ray diffraction (PW1710 Philips) with CrKα radiation ($\lambda = 2.2897$ Å). The surface morphology and grain size of sintered powders were studied by scanning electron microscopy (SEM: Model JEOL-JSM6360). The grain size of all samples was calculated by Cottrell's method while elemental contents were determined using an energy dispersive X-ray spectroscopy (EDAX). The room temperature magnetic measurements for all the compositions were performed by using a computerized high field hysteresis loop tracer (Magenta, Mumbai) at the magnetic field strength of 2.5 kOe.

The lattice parameters were calculated for the cubic phase using following relations.

$$\frac{1}{d^2} = \frac{h^2 + k^2 + l^2}{a^2} \quad (1)$$

where a = lattice parameter; $(h\,k\,l)$ = Miller indices and d = interplanar distance.

The crystallite size was estimated using Scherrer's formula.

$$t = \frac{0.9\lambda}{\beta \mathrm{Cos}\,\theta} \quad (2)$$

where symbols have their usual meaning.

* Corresponding author. Tel.: +91 231 2609381.
E-mail address: p_hankarep@rediffmail.com (P.P. Hankare).

0925-8388/$ – see front matter © 2010 Published by Elsevier B.V.
doi:10.1016/j.jallcom.2010.03.178

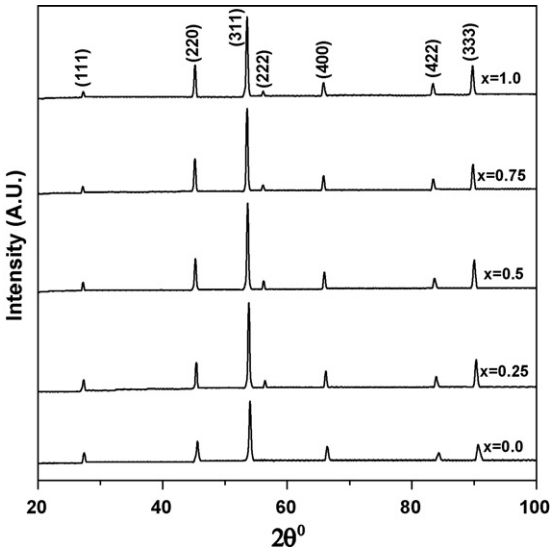

Fig. 1. X-ray diffraction patterns of $Cu_{1-x}Zn_xFe_2O_4$ ferrites with $x = 0.0$, 0.25, 0.5, 0.75, 1.0.

The actual density (d_x) was calculated according to the formula

$$d_x = \frac{8M}{Na^3} \quad (3)$$

where 'M' is the molecular mass, 'N' is the Avogadro's number, and 'a' is the lattice parameter.

The percentage porosity of sample was calculated using the formula

$$P(\%) = \left(\frac{d_x - d_a}{d_x}\right) \times 100 \quad (4)$$

where d_x = actual density and d_a = theoretical density.

3. Results and Discussion

3.1. X-ray diffraction analysis

Fig. 1 shows X-ray diffraction patterns of ferrite samples $Cu_{1-x}Zn_xFe_2O_4$ ferrites with $x = 0.0$, 0.25, 0.5, 0.75 and 1.0. The diffraction patterns confirm that, the single cubic phase is formed in all the samples. The lattice parameter increases with increasing Zn content as shown in Fig. 2., which is attributed to the fact that ionic radius of Zn^{2+} ion (0.83 Å) is greater than that of Cu^{2+}(0.70 Å) [11]. Similar results were observed by Lipare et al. [12] and Mazen et al. [13]. The actual density decreases with substitution of zinc content. This confirms the observation that, the addition of zinc in copper ferrites results in the lowering of density of the material. The theoretical density of the ferrites was determined accurately by the hydrostatic method. Plot of therotical density vs. zinc content is shown in Fig. 3. It can be seen from the figure that the theoretical density increases up to $x = 0.5$ and there after decreases with further increase of Zn content. The data on Lattice constant (a), crystallite size (t), actual density (d_x), theoretical density (d_a) and percentage porosity (P) for the samples is listed in the Table 1.

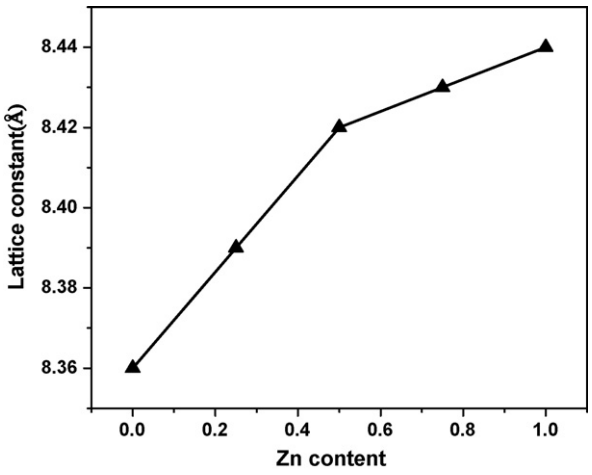

Fig. 2. Variation of lattice parameters with Zn content.

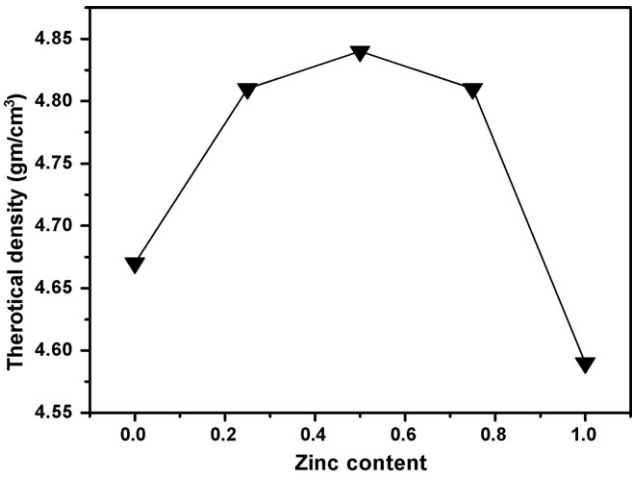

Fig. 3. Variation of theoretical density Zn content.

3.2. Scanning electron microscopy

The SEM micrographs of the samples are shown in the Fig. 4(a–e). The study reveals that, all the samples show fine grains. The average grain size was calculated by Cottrell's method [14]. The average grain size lies in the range 0.267–1.058 μm. The average grain size of ferrite increases up to $x = 0.5$ and later on decreases with further increase in x. From the micrograph, it is observed that the porosity decreases with increasing grain size.

3.3. Energy dispersive X–ray spectroscopy

The chemical composition of the products was determined by EDAX spectra analysis shown in Fig. 5(a–c). The spectra show the presence of Cu, Zn, Fe, and O in the samples and do not contain

Table 1
Data on lattice constants, crystallite size, actual density, theoretical density and porosity for $Cu_{1-x}Zn_xFe_2O_4$ samples.

Sr. no.	Composition (x)	Lattice constant (a) (Å) ±0.01	Crystallite size (t) (nm) ±0.01	Actual density (d_x) gm/cm^3	Theoretical density (d_a) gm/cm^3	Porosity (P) (%)
1	0.0	8.36	37.34	5.43	4.67	14.0
2	0.25	8.39	47.10	5.39	4.81	10.7
3	0.5	8.42	47.60	5.34	4.84	9.4
4	0.75	8.43	46.72	5.33	4.81	9.7
5	1.0	8.44	45.59	5.33	4.59	13.8

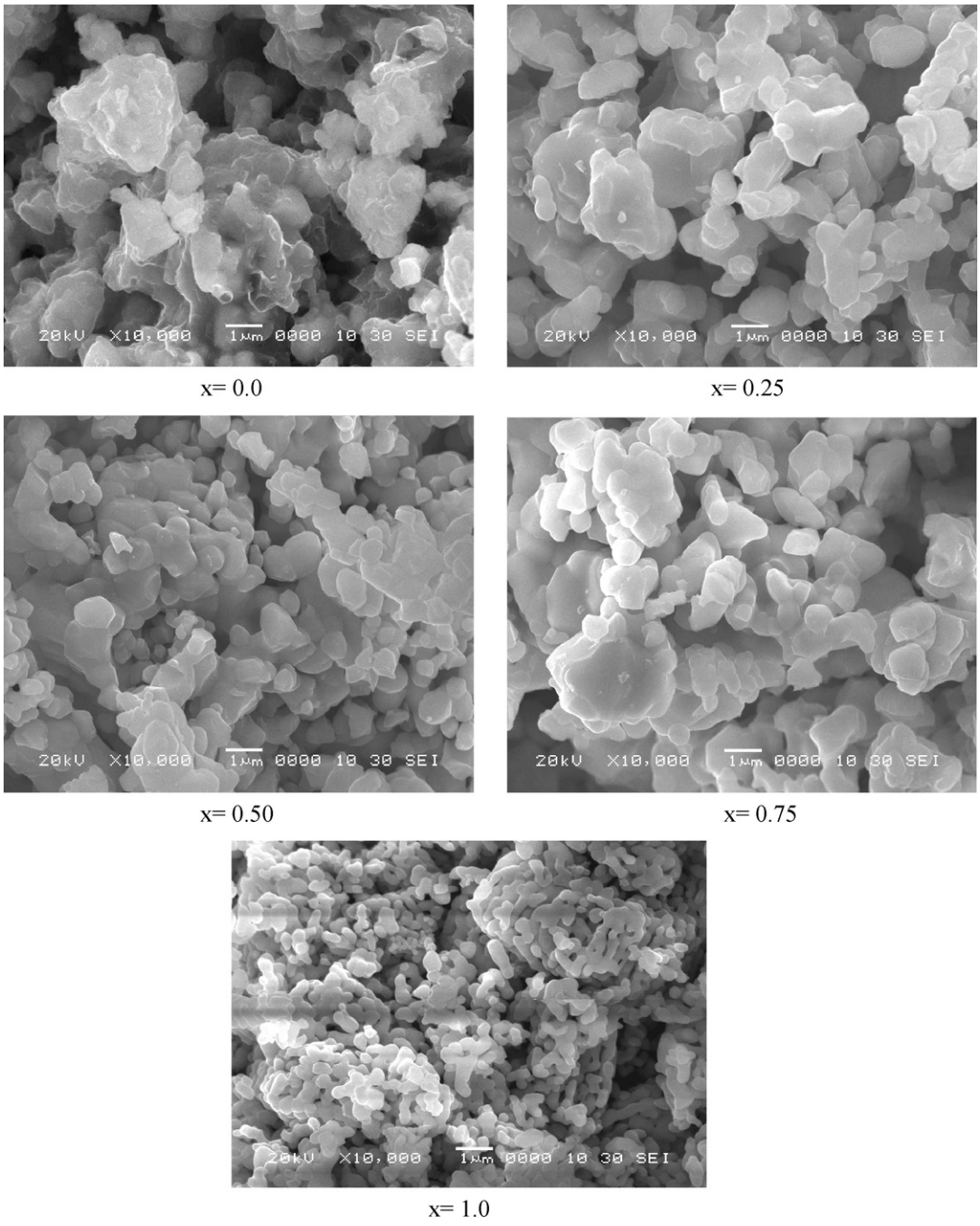

Fig. 4. Scanning electron micrographs of $Cu_{1-x}Zn_xFe_2O_4$ samples with $x = 0.0, 0.25, 0.5, 0.75, 1.0$.

Table 2
Elemental analysis of $Cu_{1-x}Zn_xFe_2O_4$ samples by EDAX.

Composition (x)	Theoretical ratio		Ratio from EDAX	
	Cu/Fe	Zn/Fe	Cu/Fe	Zn/Fe
0.0	0.5	–	0.452	–
0.5	0.25	0.25	0.222	0.235
1.0	–	0.5	–	0.464

any other elemental impurities. The results indicate that, the cation impurities do not take part in the reaction. The average atomic ratios of Cu/Fe and Zn/Fe were calculated theoretically from the spectra and are listed in the Table 2.

3.4. Magnetic hysteresis

Fig. 6 shows the magnetic hysteresis loops for the samples. The hysteresis parameter such as saturation magnetization (M_s), remanant magnetization (M_r), coercive field (H_c) and magnetic moment (μ_B) are listed in Table 3. The saturation magnetization increases up to $x = 0.5$ and there after decreases as shown in Fig. 7.

The magnetic moment per formula unit in Bohr magneton (μ_B) was calculated by using the relation [15].

$$\mu_B = \frac{MW \times M_S}{5585} \quad (5)$$

where MW = molecular weight of composition (in grams); M_S = saturation magnetization (in Oe).

Table 3
Data on magnetic hysteresis for $Cu_{1-x}Zn_xFe_2O_4$ system.

Sr. no	Samples	Saturation magnetization (M_s) at 250 K (emu/gm)	Coercive field (H_c) (Oe)	Remanent magnetisation (M_r) (emu/gm)	Magnetic moment (μ_B) Bohr magnetons
1	$CuFe_2O_4$	8.90	225.3	1.89	0.38
2	$Cu_{0.75}$ $Zn_{0.25}Fe_2O_4$	10.87	190.63	3.54	0.47
3	$Cu_{0.5}$ $Zn_{0.5}Fe_2O_4$	17.53	156.32	5.38	0.75
4	$Cu_{0.25}$ $Zn_{0.75}Fe_2O_4$	13.81	159.45	2.99	0.59
5	$ZnFe_2O_4$	2.37	390.26	1.05	0.10

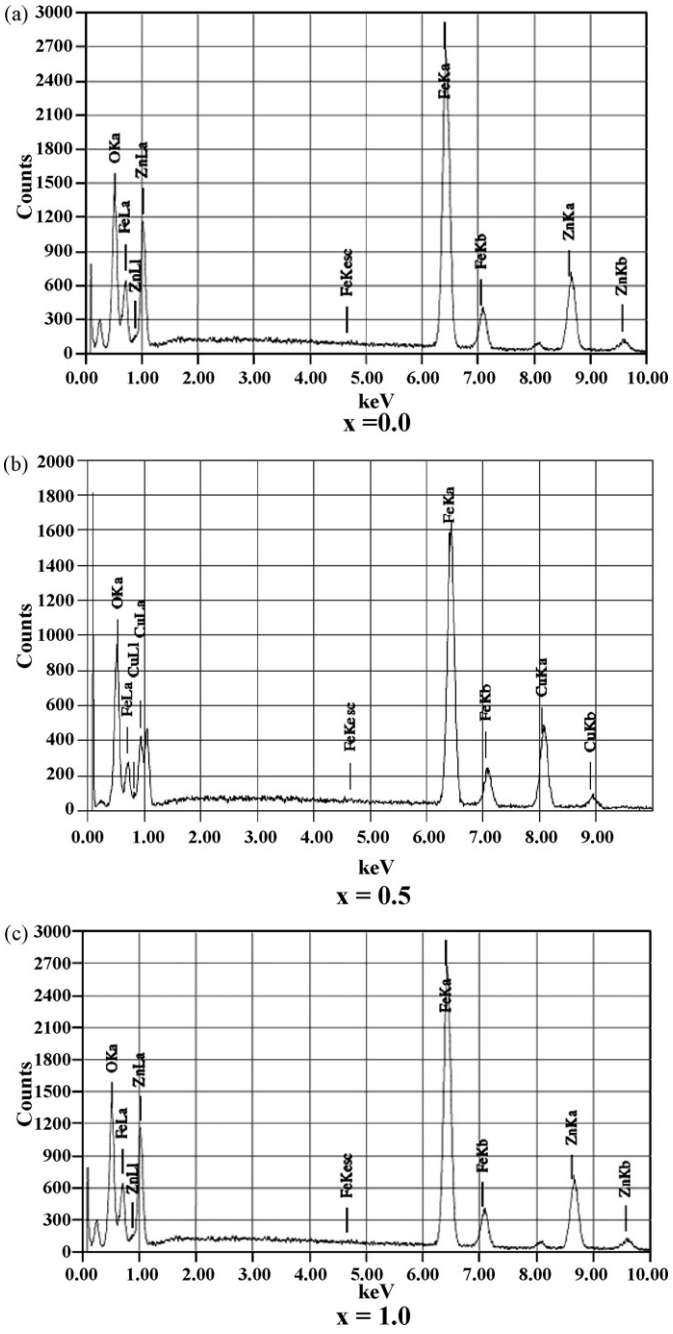

Fig. 5. EDAX spectra of $Cu_{1-x}Zn_xFe_2O_4$ samples.

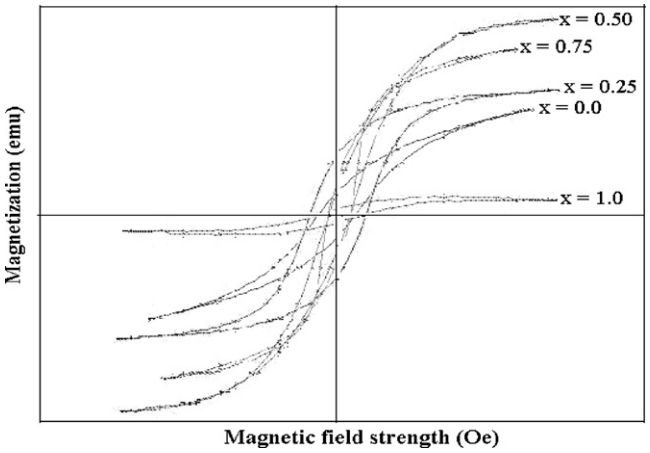

Fig. 6. Hysteresis loops for $Cu_{1-x}Zn_xFe_2O_4$ samples.

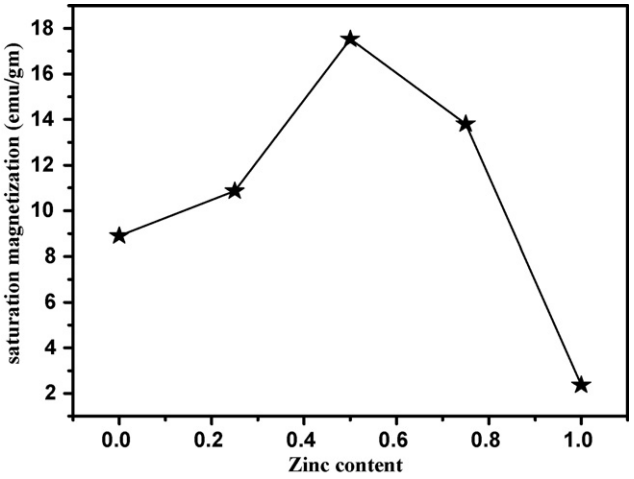

Fig. 7. Variation of saturation magnetisation (M_s) with zinc content.

The Zn^{2+} ions occupy tetrahedral A-site and Cu^{2+} ions are distributed over the tetrahedral A and octahedral B-sites. Due to non-magnetic substitution of Zn^{2+} ions at tetrahedral A-sites magnetic moment decreases [16,17] Similarly due to the substitution of Cu^{2+} ions at tetrahedral (A) and octahedral (B) sites in place of Fe^{3+} ions, the magnetic moment of octahedral B-site also decreases. However, A-site magnetic moment is less than B-site magnetic moment for all the compositions. The net magnetic moment (μ_B) increases initially up to $x = 0.5$ and then decreases with further increase in Zn content due to Yafet and Kittel spin arrangement [18].

4. Conclusion

A series of Zn-substituted copper ferrite powders were successfully synthesized by oxalate co-precipitation method. X-ray diffraction patterns reveal the single cubic structure of all the samples. Scanning electron micrographs indicate the increase in grain size up to $x = 0.5$ and later on it decreases with Zn content. The contents of the metals in the resulting spinel ferrites are close to the theoretical values as shown by EDAX measurements. Magnetic

hysteresis measurements indicate that, all the compositions are ferrimagnetic in nature. The saturation magnetization increases with Zn content upto $x = 0.5$ and then it decreases due to Yafet and Kittel spin arrangement on the B-site.

Acknowledgement

Author (PPH) is very thankful to DAE-BRNS, Mumbai for financial assistance through Major research project No. 2009/37/41/BRNS/2231.

References

[1] S.C. Watanabe, S.P. Bamne, S.P. Tangsali, Mater. Chem. Phys. 103 (2007) 323.
[2] J.R. Dahn, U. Vomsacken, C.A. Micha, Solid State Ionics 44 (1990) 87.
[3] G.M. Argentina, P.D. Baba, IEEE Trans. Microwave Theory Tech. MTT 22 (1974) 652.
[4] P.P. Hankare, R.P. Patil, U.B. Sankpal, S.D. Jadhav, P.D. Lokhande, K.M. Jadhav, R. Sasikala, J. Solid State Chem. 182 (2009) 3217.
[5] Mazhar U Rana, Misbah-ul Islam, Tahir Abbas, Mater. Chem. Phys. 65 (2000) 345.
[6] Mazhar U. Rana, Tahir Abbas, J. Magn. Magn. Mater. 246 (2002) 110.
[7] H.A. Dawond, S.K.K. Shaat, The ISLA Univ. J. (Ser. Nat. Studies Eng.) 14 (2006) 165.
[8] J. Kulikowski, J. Magn. Mater. 41 (1984) 56.
[9] P. Ravindranathan, K.C. Patil, Mater. Sci. 22 (1987).
[10] P.P. Hankare, M.R. Kadam, P.D. Kamble, K.S. Rane, P.N. Vasambekar, Mater. Lett. 61 (13) (2007) 2769.
[11] R.D. Shannon, C.T. Prewitt, Acta Crystallogr. B26 (1970) 1076.
[12] A.Y. Lipare, P.N. Vasambekar, A.S. Vaigankar, Bull. Mater. Sci. 26 (2003) 493.
[13] S.A. Mazen, S.F. Mansor, H.M. Zaki, Cryst. Res. Technol. 38 (6) (2003) 472.
[14] A. Cottrell, An Introduction to Metallurgy, Edward Arnold, London, 1967.
[15] Jan Smit, Book of Magnetic Properties of Materials, Intra-University Electronics Series, 13, McGraw-Hill Book Co., New York, 1971, 89.
[16] F.N. Kong, 10th International Conference on Ground Penetrating Radar, Delft, Netherlands, 2004.
[17] M.R. Anantharaman, S. Jagatheesan, K.A. Malini, S. Sindhu, A. Sarayanasamy, C.N. Chennasarry, J.P. Jacob, S. Reijne, J. Magn. Magn. Mater. 189 (1998) 83.
[18] Y. Yafet, C. Kittel, Phys. Rev. 90 (1952) 295.